Supporting Information

Structure and topology of the huntingtin 1-17 membrane anchor by a combined solution and solid-state NMR approach

Matthias Michalek, Evgeniy S. Salnikov, and Burkhard Bechinger*

[1]Université de Strasbourg / CNRS, UMR7177, Institut de Chimie, 1, rue Blaise Pascal, 67070 Strasbourg, France

* corresponding author: Burkhard Bechinger
1, rue Blaise Pascal, 67070 Strasbourg, France
Tel.: +33 3 68 85 13 03, FAX: +33 3 68 85 17 35, bechinger@unistra.fr

Supplementary Table 1: Structural statistics of the 20 energetically lowest, independently calculated structures of huntingtin 1-17 in 100 mM DPC-d_{38} and in 50% (v/v) TFE-d_3. Pair-wise r.m.s. deviations were calculated among 20 refined structures.

Distance constraints	**DPC**	**TFE**
Total NOE	108	116
Intra-residue	44	43
Sequential (|i-j| = 1)	39	40
Medium-range (|i-j| < 4)	25	33
Structure statistics		
Violations (mean and s.d.)		
Distance constraints (Å)	0.025 ± 0.002	0.014 ± 0.001
Max. dist. constraint violation (Å)	0.450	0.180
Deviations from idealized geometry		
Bond lengths (Å)	0.019 ± 0.0002	0.018 ± 0.0001
Bond angles (°)	0.839 ± 0.017	0.602 ± 0.018
Impropers (°)	0.932 ± 0.035	0.592 ± 0.050
Average pairwise r.m.s. deviation (Å)		
Heavy (all residues)	2.068 ± 0.57	1.671 ± 0.20
Backbone (all residues)	1.573 ± 0.53	1.12 ± 0.21
Heavy (residue 6-16)	0.902 ± 0.10	0.858 ± 0.16
Backbone (residue 6-16)	0.238 ± 0.09	0.188 ± 0.10
Ramachandran plot (%)		
Most favored regions	81.3	75.0
Additionally allowed regions	17.3	23.7
Generously allowed regions	1.0	1.3
Disallowed regions	0.3	0

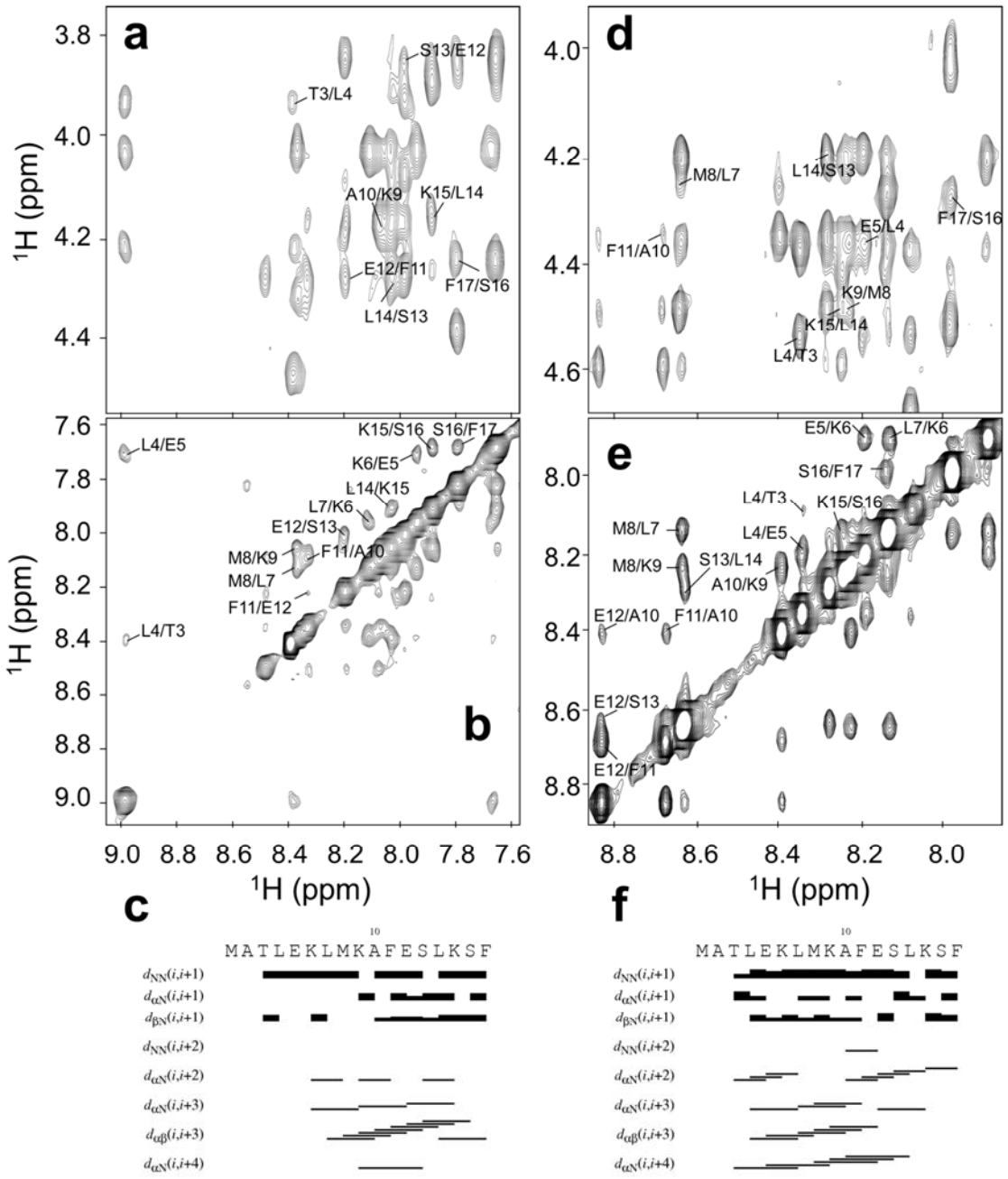

Figure S1: ^{1}H-^{1}H-NOESY fingerprint (Hα-HN) and amide (HN-HN) region of 0.5 mM huntingtin 1-17 in 100 mM DPC-d_{38} (a,b) and in TFE/buffer 50/50 v/v (**d,e**) at mixing times of 200 ms. The assignments of the interresidual correlations are indicated. (**c,f**) Graphical summary of the NOE constraints obtained from multidimensional solution NMR spectroscopy of 0.5 mM huntingtin 1-17 in the presence of 100 mM DPC-d_{38}, pH 6.0 (**c**) and in TFE/buffer 50/50 v/v, pH 7.4 (**f**) at 25 °C. The thickness of lines represents strong, medium and weak NOE intensities, respectively.

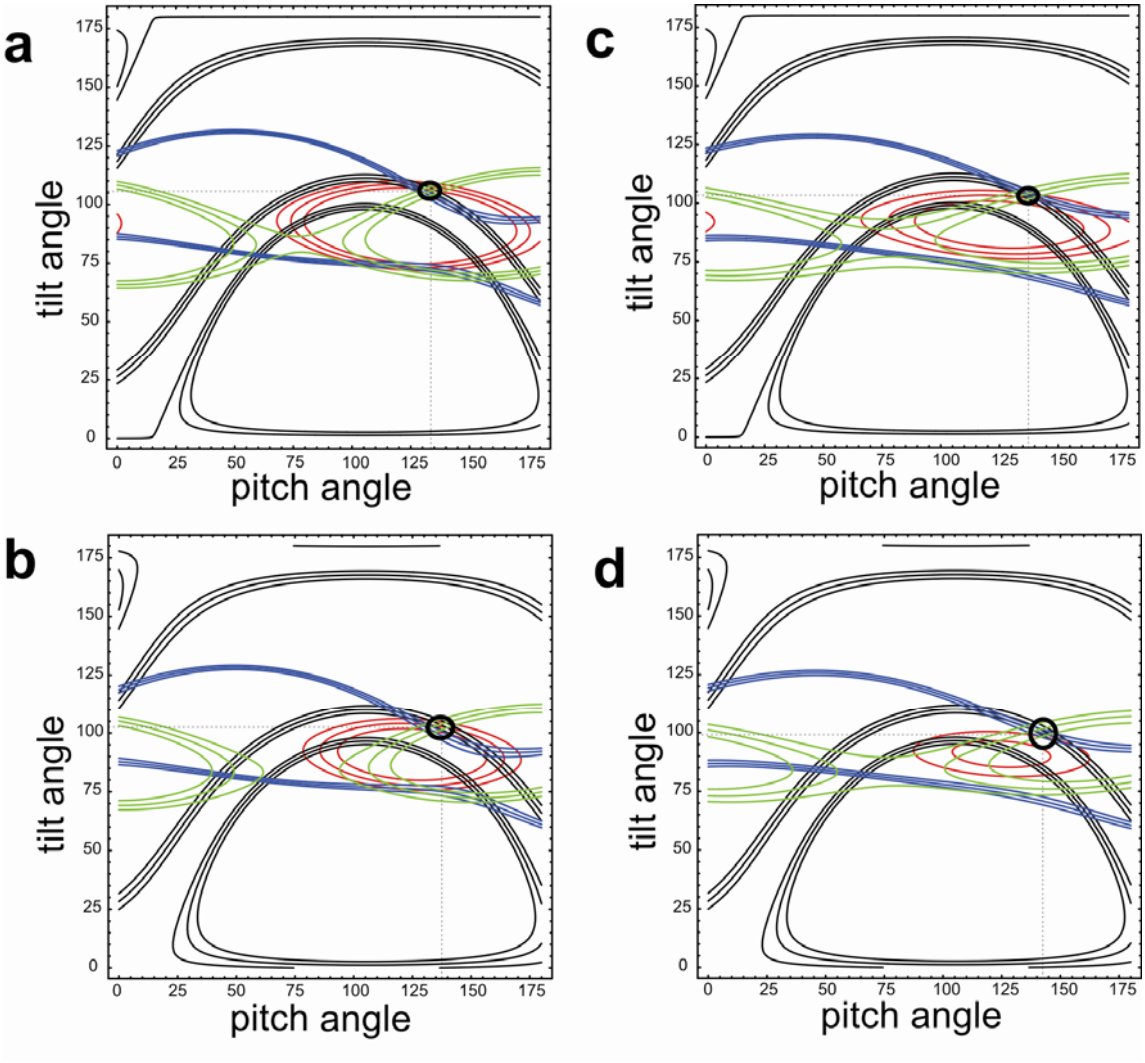

Figure S2: Angular restrictions obtained from oriented solid-state NMR spectra shown in Figure 4 a,c,e and g also used for the calculations shown in Figure 5. Here an analysis of systematic errors is performed by variation of the main tensor elements as well as modifications of the motions that lead to spectral averaging. The possible alignments of the low-energy conformer 3 obtained from the solution NMR structural analysis in the presence of DPC micelles (Figure 2) are represented by their helical tilt and the rotational pitch angles. The solid black lines represent angular pairs that agree with the experimental ^{2}H quadrupolar splitting obtained from $^{2}H_{3}$-Ala^{10} (11 ± 2.5 kHz), the ^{15}N chemical shifts of ^{15}N-Leu^{7} (red; 71.5 ± 2.5 ppm), ^{15}N-Phe^{11} (green; 78.5 ± 3 ppm) and ^{15}N-Phe^{17} (blue; 88 ± 1.7 ppm). The tilt/rotational pitch angular pairs where all the experimental measurements agree or come close are circled. Restriction plots obtained when using the ^{15}N main tensor elements (56, 81, 223 ppm) are shown in **a** and **b**, those using the tensor (64, 77, 217 ppm) in **c** and **d**. Panels **a** and **c** assume a static peptide whereas **b** and **d** were calculated with wagging fluctuations of the peptide orientations within a 10º Gaussian distribution and azimuthal fluctuations of 18º (similar to Figure 5).

In order to test in a systematic manner how motions and/or uncertainties in the main tensor elements affect the topological analysis additional calculations were performed (Figure S2). For these calculations tensor values that correspond to an average of the published values for peptide bonds were used (1). Alternatively, the calculations were performed with a published tensor that is within the range of experimentally obtained values (1). but which has a maximal effect on the topological analysis. Furthermore, fluctuations around the helix long axis and wagging motions of the latter were simulated by Gaussian distribution functions similar to those that have been shown to provide best agreement of the ^{2}H solid-state NMR restraints of an amphipathic helix of similar dimensions (2). As a consequence of these uncertainties the tilt/pitch angles of conformer 3 varied between 98º /142º and 107º/132º. Importantly, in all calculations all four solid-state NMR orientational restraints fit to an alignment of conformer 3 which was one of 20 low-energy structures calculated from the solution NMR conformational restraints obtained in the presence of DPC micelles.

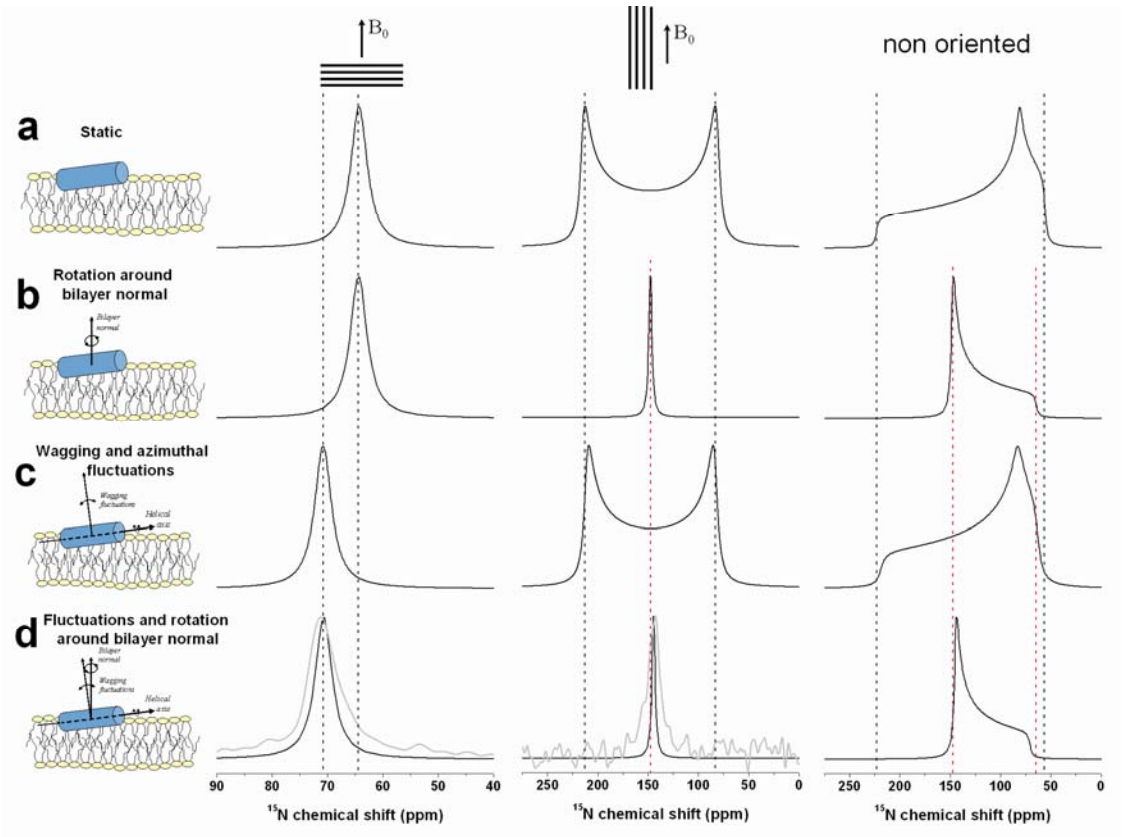

Figure S3: Simulation of the effects of motions on the ^{15}N –solid-state NMR spectra of [^{15}N-Leu^{7}]-huntingtin 1-17. The underlying topology is that obtained from the analysis of experimental spectra (helix tilt /pitch angle 103º/137º; Figures 5 and S2). Row **a** shows the spectra that are obtained in the absence of motions. Row **b** shows spectra that result from fast rotational diffusion around the bilayer normal. Row **c** illustrates the influence of wagging and azimuthal fluctuations with 10º and 18º Gaussian distribution, respectively. The effect of both motions and rotation around the bilayer normal is shown in row **d**. Please note the different scale in the first column. Row **d** agrees with the experimental measurements of 71 ppm (Figure 4e) and 144 ppm (Figure 4f) for sample alignments with the normal parallel and perpendicular to B_o, respectively. The discontinuities of the powder pattern sample shown in the last column reflect these values (3).

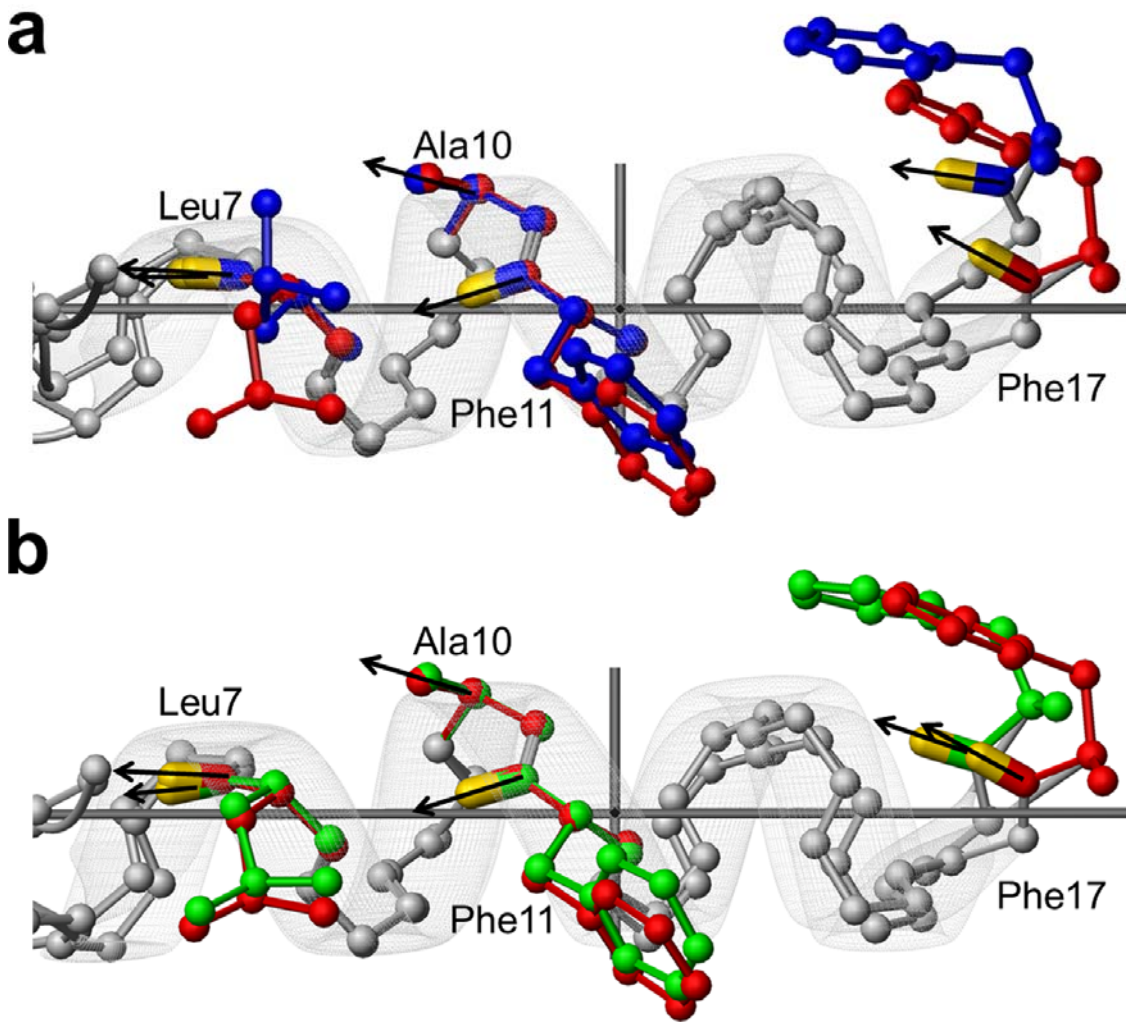

Figure S4: Structural details of huntingtin 1-17 for conformer 3 (red) are compared to conformer 1 (blue) (a) and conformer 20 (green) (b). The labeled sites used for the topological analysis are highlighted by stick and ball models and arrows, the ^{15}N-^{1}H vectors are highlighted in yellow. The conformers 3 and 20 show good agreement with the topology and orientation of the labeled sites, whereas conformer 1 represents a structure that does not match the solid-state NMR topological analysis.

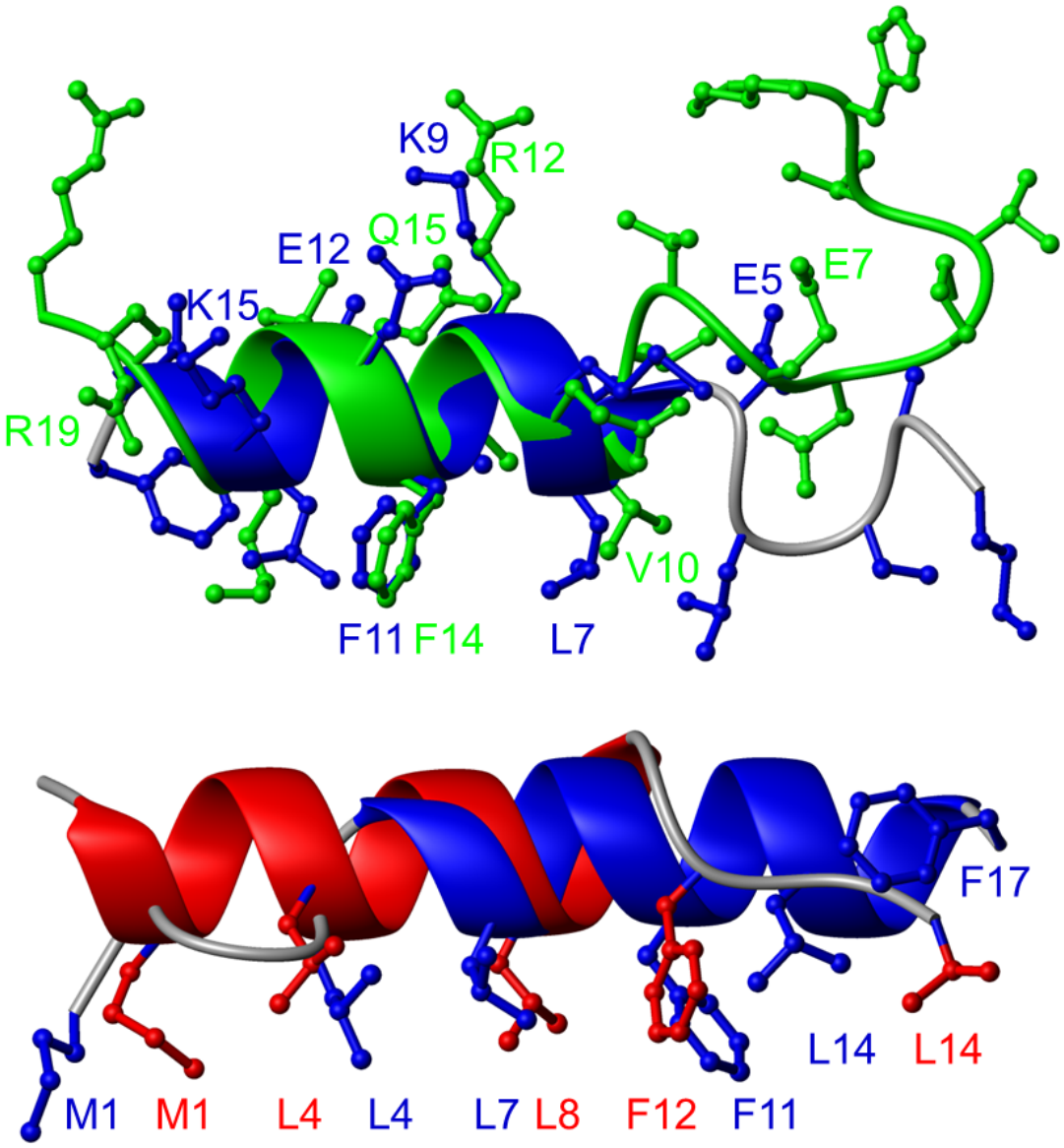

Figure S5: Comparison of the huntingtin 1-17 structure in DPC micelles (blue; pdb 2LD2) with the F-actin binding sequence of gelsolin (green; pdb 1SOL; residues 150-169) and the nuclear export signal of snurportin 1 (SPN1; red; pdb 3GJX). Whereas the latter is taken from the structure of the amino-terminal part of SPN 1 in the complex of SPN1 with CMB1 and RanGTP (4), the gelsolin peptide was investigated in TFE/water 50/50 v/v (5). For orientation the amino-acid residues with similar characteristics are assigned in their respective color.

SUPPORTING REFERENCES

1. Salnikov, E., P. Bertani, J. Raap, and B. Bechinger. 2009. Analysis of the amide (15)N chemical shift tensor of the C(alpha) tetrasubstituted constituent of membrane-active peptaibols, the alpha-aminoisobutyric acid residue, compared to those of di- and tri-substituted proteinogenic amino acid residues. J Biomol NMR 45:373-387.
2. Strandberg, E., S. Esteban-Martin, J. Salgado, and A. S. Ulrich. 2009. Orientation and dynamics of peptides in membranes calculated from 2H-NMR data. Biophys J 96:3223-3232.
3. Salnikov, E., C. Aisenbrey, V. Vidovic, and B. Bechinger. 2010. Solid-state NMR approaches to measure topological equilibria and dynamics of membrane polypeptides. Biochim. Biophys. Acta 1798:258-265.
4. Monecke, T., T. Guttler, P. Neumann, A. Dickmanns, D. Gorlich, and R. Ficner. 2009. Crystal Structure of the Nuclear Export Receptor CRM1 in Complex with Snurportin1 and RanGTP. Science 324:1087-1091.
5. Xian, W. J., R. Vegners, P. A. Janmey, and W. H. Braunlin. 1995. Spectroscopic studies of a phosphoinositide-binding peptide from gelsolin: Behavior in solutions of mixed solvent and anionic micelles. Biophys J 69:2695-2702.